Blood Pressure Estimation From Korotkoff Sound Signals Using an End-to-End Deep-Learning-Based Algorithm

Ahmadreza Argha, *Member, IEEE*, Branko G. Celler, *Life Fellow, IEEE*, Hamid Alinejad-Rokny, *Member, IEEE*, and Nigel H. Lovell, *Fellow, IEEE*

***Abstract*— While measurement of blood pressure (BP) is now widely carried out by automated noninvasive BP (NIBP) monitoring devices, as they do not require skilled clinicians and do not carry the risk of complications, their accuracy is in doubt. A novel end-to-end deep-learning-based algorithm was developed in this study that estimates NIBP directly from sequences of Korotkoff sounds (KSs) rather than oscillometric waveforms (OWs). First, sequences of segments of KSs were formed using different signal segmentation techniques, that is, segmentation using a sliding window with or without overlap and segmentation using the cardiac period estimation. Each segment within each sequence was then labeled as 1) after-systolic and before-diastolic (AB) or 2) before-systolic or after-diastolic (BA) such that a binary sequence-to-sequence classification problem was achieved. To deal with the resultant sequence-to-sequence classification problem, an algorithm was developed by combining 1-D convolutional neural networks (CNNs) and recurrent neural networks (RNNs). The segments associated with systolic and diastolic BP (SBP and DBP) are then identified as the segments at which the output target sequence switches from class BA to class AB and later from class AB to class BA. Lastly, the values of SBP and DBP are obtained by mapping the center point of the switching segments to the deflation curve. To evaluate the performance of the proposed NIBP estimation method, we used a database of 350 NIBP samples collected from 155 participants (87 males, age: 23–97 years, arm circumference: 10–35 cm, SBP: 81–104 mmHg, and DBP: 37–104 mmHg), and the achieved estimation errors for SBP and DBP, relative to the reference values, using a fivefold cross-validation approach, were 1.6 ± 3.9 mmHg (mean absolute error ± standard deviation of error) and 2.5 ± 4.0 mmHg, respectively. We finally conclude that the proposed end-to-end deep-learning-based NIBP estimation algorithm from sequences of KSs is a novel technique that requires modest preprocessing steps and can measure BP accurately.**

***Index Terms*— Auscultatory noninvasive blood pressure (NIBP) monitoring devices, combined convolutional neural networks (CNNs) and bidirectional long short-term memory recurrent neural networks (LSTM-RNNs), deep-learning-based NIBP estimation, Korotkoff sounds (KSs), noninvasive systolic and diastolic BP (SBP and DBP) estimation.**

I. Introduction

HYPERTENSION, the leading modifiable risk factor for cardiovascular disease, affects more than one billion people globally and kills 10.4 million people every year [1]. Hence, the management and treatment of hypertension, as a significant global health burden, is now demanding concerted action embracing basic science and clinical and social aspects. In addressing the impact of hypertension across the life-course of cardiovascular health, the Lancet Commission on Hypertension [2] has identified improved accuracy of blood pressure (BP) measurement as one of the key actions, requesting "better quality of BP measurement through endorsed protocols and certified and validated BP monitors."This has already promoted action on understanding the current deficiencies in BP measurement [3], [4] and unifying regulatory procedures for device validation [5].

Continuous invasive BP is a very important vital sign monitored during the management of critically ill patients. To measure BP invasively, a catheter is inserted into the radial artery, and as a result, it must be carried out by a skilled clinician. Nevertheless, this still can put patients at different risks such as ischemia, infection, and bleeding [6]. As a result, noninvasive BP (NIBP) monitoring devices are now widely used to measure BP. The accepted gold standard for NIBP measurement is auscultatory sphygmomanometry [7], [8] whereby a cuff is placed over the upper arm and inflated to supra systolic BP (SBP) to ensure that the brachial artery is fully occluded. A stethoscope placed under the occluding cuff and over the brachial artery is used to detect the Korotkoff sounds (KSs) during cuff deflation where systolic and diastolic BP (DBP) correspond to the appearance and disappearance of the KSs, respectively. However, this long-standing auscultatory method is giving way to automated methods for NIBP measurement using the oscillometric method [9], [10], where SBP and DBP are determined by proprietary algorithms analyzing the envelope of the cuff pressure oscillations during cuff deflation, namely oscillometric waveform envelope (OWE).

The main focus of conventional oscillometric methods has been on the OWE, and several conventional algorithms, including the maximum amplitude algorithm (MAA) [11] and the maximum/minimum slope algorithm (MMSA) [12],

Manuscript received 19 June 2022; revised 20 September 2022; accepted 9 October 2022. Date of publication 28 October 2022; date of current version 9 November 2022. The Associate Editor coordinating the review process was Dr. Lin Xu. *(Corresponding author: Ahmadreza Argha.)*

This work involved human subjects or animals in its research. Approval of all ethical and experimental procedures and protocols was granted by the Research Ethics Committee of UNSW under Approval No. 12/11.

Ahmadreza Argha and Nigel H. Lovell are with the Graduate School of Biomedical Engineering, the Tyree Institute of Health Engineering (IHealthE), and Ageing Futures Institute, UNSW Sydney, NSW 2052, Australia (e-mail: a.argha@unsw.edu.au; n.lovell@unsw.edu.au).

Hamid Alinejad-Rokny is with the Graduate School of Biomedical Engineering, UNSW Sydney, NSW 2052, Australia (e-mail: h.alinejad@unsw.edu.au).

Branko G. Celler is with the School of Electrical Engineering and Telecommunications, UNSW Sydney, NSW 2052, Australia (e-mail: b.celler@unsw.edu.au).

Digital Object Identifier 10.1109/TIM.2022.3217865

have been proposed to estimate SBP and DBP from OWE. It was recently noted that the oscillometric pulses are also very informative, and thus, efforts have been made to develop algorithms to estimate SBP and DBP from the oscillometric pulses. This approach estimates the NIBP values by modeling the oscillometric pulses or by measuring and processing the changes in oscillometric pulse morphology [13].

The majority of the proposed artificial intelligence (AI)-based NIBP estimation algorithms in the literature use oscillometric waveforms (OWs), and more specifically, they have mimicked the classical MAA. In other words, these AI-based algorithms estimate the ratios corresponding to SBP and DBP using features extracted from OWE, and via different AI-based algorithms, such as Gaussian mixture models (GMMs) and Gaussian mixture regression (GMR), and deep-learning regression methods [9]. Recently, different AI-based NIBP estimation approaches have been developed in which SBP and DBP are estimated using a classification problem formed to classify feature vectors extracted from pulses of oscillogram. Several AI-based classification methods were used to estimate NIBP using oscillometric pulses. These classification-based methods can be divided into two major categories based on their ability to take into account the dependencies between the neighboring pulses, for example, long short-term memory recurrent neural networks (LSTM-RNNs) [14] and hidden Markov models (HMMs) [15] versus deep-belief-network deep-neural networks (DBN-DNNs)- and feedforward neural networks (FFNNs)-based classification models [16].

Cuff-less NIBP monitoring methods are beginning to emerge as a popular modality for NIBP estimation. These devices can be very useful for hypertension awareness, management, and control. However, there are currently serious problems with the accuracy of cuff-less NIBP monitoring devices, and the 2021 European Society of Hypertension Guidelines on BP measurement do not recommend them for clinical use [17].

A. Study Motivations

Oscillometric NIBP measurements are also generally considered less accurate than auscultatory measurements [18], [19], and the oscillogram can be disturbed by cardiac arrhythmia, frequently present in elderly patients aged >65 with chronic conditions [20], [21]. To estimate NIBP directly from KSs and further assess the accuracy of the marketed oscillometric NIBP monitoring devices, a number of smartphone-based kits have been introduced [22], [23]. On the other hand, numerous studies have demonstrated that there are significant differences between readings of different operators carrying out BP measurements using sphygmomanometry [24], [25]. This indicates the necessity to develop automated auscultatory techniques which are less operator-dependent. The study in [26] proposed the so-called K_2 algorithm which, in fact, is a visual technique to estimate SBP and DBP more accurately than the auscultation technique. This is because the visual method can detect the appearance and disappearance of K_2 (higher frequency, that is, $\geq$20 Hz, components of KSs) even if KSs are inaudible. The K_2 method eliminates the need for *listening* to KSs, which has been shown to be dependent on the operator's hearing acuity, the sensitivity of the stethoscope, and the particular morphometry of the signal. However, decisions still need to be made to determine the onset and end of K_2 sounds. This is not a straightforward problem, and the K_2 algorithm cannot be automated using simple thresholding techniques, due to the presence of noise in the digitized signal. So, the K_2 algorithm at best is a semiautomated algorithm and still requires human intervention to detect the systolic and diastolic beats. A possible solution is to use AI, and especially deep learning, methods. AI-based methods proposed for NIBP estimation from KSs can be summarized as: 1) methods that ignore the temporal dependencies between the segments derived from KSs [27], [28], [29] and classify each pulse independent of others; and 2) methods that consider the digitized KSs as time series and estimate BP from sequences of KSs through dealing with a sequence-to-sequence (seq-to-seq) classification problem using classification algorithms, such as HMM [15], [30] and LSTM-RNN [31].

B. Contributions to the Field

In this study, a novel end-to-end deep-learning-based technique was developed to accurately estimate NIBP from KSs, which requires modest preprocessing and belongs to the latter category discussed above. This approach converts the NIBP estimation from the digitized KSs to a seq-to-seq classification problem using two segmentation techniques that can segment the KSs without having a parallel OW. This is unlike the existing methods proposed for forming seq-to-seq classification problems [27], [30], [31] that require a parallel OW. Additionally, we developed and used a combination of convolutional neural networks (CNNs) and bidirectional LSTM-RNNs (BiLSTM-RNNs), namely CNN-BiLSTM-RNNs, to classify segments derived via the segmentation techniques. This can classify segments derived from KSs considering other (previous and future) segments, so can effectively deal with noise in KSs which happens before systolic or after diastolic points. This approach is also different from the current methods that use manual feature extraction techniques (cf. [30], [31]) and requires less preprocessing steps to process the raw KSs and extract suitable inputs (features) for the seq-to-seq classification algorithm.

II. Methods

A. Validation Protocols and Gold Reference

A number of regulatory agencies and standards organizations have introduced protocols for validation of NIBP monitoring devices, such as the U.S. Association for the Advancement of Medical Instrumentation (AAMI) [32], the British Hypertension Society (BHS) [33], and the International Organization for Standardization (ISO). A device passes the ANSI/AAMI/ISO protocol introduced by the ANSI (American National Standards Institute), the AAMI along with the ISO, if the achieved absolute value of mean error (ME) and standard

deviation of the error (SDE) over the dataset are, respectively, $\leq$5 and $\leq$8 mmHg. The BHS standard [33], on the other hand, categorizes the NIBP monitoring devices based on the percentages of the absolute values of the error being less than 5, 10, and 15 mmHg. In 2018, a consensus document was jointly published by all the standards bodies with the intention of releasing a single AAMI/ESH/ISO standard that will replace all other previous standards and protocols. Based on this universal standard that is now available as ISO 81060-2:2018 [5], a device is acceptable if the error of $\geq$85% of its estimations is less than or equal to a tolerable value (10 mmHg).

Despite the differences between these protocols, a common thread is the use of manual auscultatory sphygmomanometry as the gold standard against which all automated NIBP devices are calibrated and validated. However, numerous studies have shown that the differences between measurements made by different observers using sphygmomanometry can be significant, especially for DBP determination [24]. The study in [26] analyzed KSs in terms of the temporal and spectral components and could detect three distinct phases (K_1, K_2, and K_3). It was also observed that the frequency spectrum of the KSs contains higher frequencies ($\geq$20 Hz) when the K_2 component is present. The study in [26] also found that the appearance and disappearance of the K_2 component are closely correlated with the pulses associated with systolic and diastolic pressures, respectively. This study further showed that the so-called K_2 algorithm [26], which, in fact, is a visual technique, can estimate SBP and DBP more accurately than the auscultation technique. This is because the visual method can detect the appearance and disappearance of K_2 even if KSs are inaudible. It should be noted that it was also shown in other studies [22], [23] that the NIBP estimates achieved using a visual technique are not significantly different from the ones achieved from the manual auscultation. In this study, to provide SBP and DBP reference values for the proposed supervised learning-based NIBP estimation method, we used a visual technique.

B. Dataset

The database (Research Ethics Committee of UNSW, Approval Number: 12/11) used in this study comprises 350 NIBP recordings collected via a single NIBP monitoring device which is a multiparameter clinical monitoring unit (CMU) from Telemedcare Pty Ltd. and has FDA approval. The CMU is merely a data collection device and its function could be replaced by a number of other devices. It is no longer in production. We used the NIBP module in its normal automated configuration. This module automatically inflates the cuff to a preset pressure and further uses a servo control to deflate the cuff at a rate of 2–3 mm per second. This device records the cuff pressure, KSs, and oscillometric signals internally between 0 and 5 V at 10-bit resolution and a sampling rate of 500 samples s^{-1} and saves it as an XML file. The methodology for collecting the data used in our article has been extensively described in [24]. Each NIBP recording contains the cuff pressure signal, the OW, and the corresponding digitized KSs. These samples were collected from 155 participants (87 males). The maximum and the minimum number of recordings per patient in this dataset are 5 and 1, respectively. The details of participants are given in Table I and can be found in [24].

TABLE I
DETAILS OF PARTICIPANTS ($n = 155$)

Male	87 (56.1%)
Female	68 (43.9%)
Age	52.0 ± 21.6 years (range 23-97)
Age (male)	51.1 ± 20.3 years
Age (female)	53.1 ± 23.4 years
Arm circumference	10-35 cm
SBP	$81 - 191$ mmHg
DBP	$37 - 104$ mmHg
MAP	$56 - 118$ mmHg

C. Preprocessing

1) High-Pass Filtering: Consistent with the process explained before for the determination of gold reference values, we high-pass filtered the KSs using a cut-off frequency of 20 Hz.

2) Root-Mean-Square Energy Calculation: The root mean square (rms) energy (RMSEn) corresponding to each KS signal was also calculated by applying a zero-phase moving average digital filter (using a Hamming window of 100 ms) to the filtered KSs. RMSEn was used in [24] as a measure of background noise and further to improve the signal-to-noise ratio of KSs. In this study, the peak locations of the RMSEn signals were detected and used as the center points around which fixed-length segments were located; see the second segmentation technique below.

3) Normalization of the KS and RMSEn Signals: Each high-pass-filtered KS signal was then standardized, that is, $z_i = (x_i - \bar{x}/SD_{x_i})$, where x_i is the ith KS sequence, $\bar{x}$ is its mean value, SD_{x_i} denotes its standard deviation, and the corresponding RMSEn was normalized to [0, 1].

D. Segmentation of the Standardized KS Signals

As shown in Fig. 1, to form the inputs to the deep-learning-based seq-to-seq classification algorithm (elaborated in the following of this section), the processed KSs were segmented using the following two methods.

1) The well-known sliding segmentation technique with or without overlap between segments [34], hereinafter called the *first* segmentation method.
2) The segments were centered with points that were detected with Algorithm 1 that estimates the cardiac period from the RMSEn signal and subsequently determines the center points around which fixed length segments were located, hereinafter called the *second* segmentation method. Note that $findPeak(\cdot, \cdot, \cdot)$ in Algorithm 1 is a subroutine that receives a signal, that is, RMSEn, and two thresholds, that is, $\alpha = 0.5$ and $\beta = 200$, and returns the indices of the peaks with a

Algorithm 1 Cardiac Period Estimation and Center Determination for the Second Segmentation Method

Input: RMSEn, root mean squared energy of the Korotkoff sound waveform
Output: CenterLocations, center points for the second segmentation technique

Initialization:

$\alpha \leftarrow 0.5$, $\beta \leftarrow 200$, $i \leftarrow 1$, $j \leftarrow 1$, $WindowSize \leftarrow 501$
PeakIndices $\leftarrow findPeak$(RMSEn, α, β)
MaxPeakIndex $\leftarrow findMax$(RMSEn)
CardiacPeriod $\leftarrow$ PeakIndices[2:end]-PeakIndices[1:end-1]
MedianCardiacPeriod $\leftarrow$ median(CardiacPeriod)
CenterLocationsRight(i) $\leftarrow$ MaxPeakIndex + MedianCardiacPeriod
$i \leftarrow i + 1$
CenterLocationsLeft(j) $\leftarrow$ MaxPeakIndex $-$ MedianCardiacPeriod
$j \leftarrow j + 1$

LOOP Process 1

while (MaxPeakIndex + $i \times$ MedianCardiacPeriod) $<$ (length(RMSEn) $-\lfloor \frac{\text{WindowSize}}{2} \rfloor$) **do**
  CenterLocationsRight(i) $\leftarrow$ MaxPeakIndex + $i \times$ MedianCardiacPeriod
  $i \leftarrow i + 1$
end while

LOOP Process 2

while (MaxPeakIndex $- j \times$ MedianCardiacPeriod) $> \lfloor \frac{\text{WindowSize}}{2} \rfloor$ **do**
  CenterLocationsLeft(j) $\leftarrow$ MaxPeakIndex $- j \times$ MedianCardiacPeriod
  $j \leftarrow j + 1$
end while

CenterLocations $\leftarrow$ concatenate(CenterLocationsLeft, MaxPeakIndex, CenterLocationsRight)
return CenterLocations

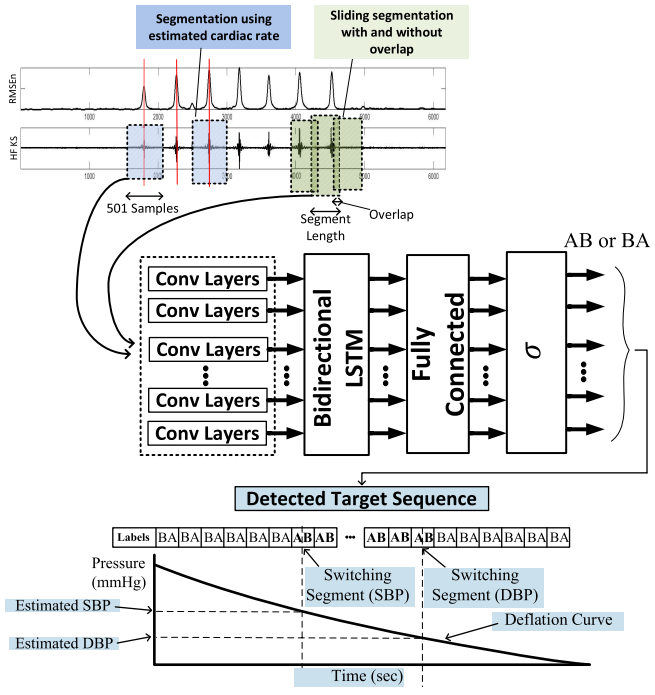

Fig. 1. Illustration of the proposed approach. Different signal segmentation methods were used to segment the high-frequency KSs, the proposed CNN-BiLSTM network to classify each segment and the method to estimate systolic and diastolic pressures through mapping the detected switching points in the detected label sequence to the corresponding cuff pressure curve.

minimum height of α and minimum distance of β samples. Also, $findMax(\cdot)$ is a subroutine that receives a signal and returns the location (index) of its maximum value.

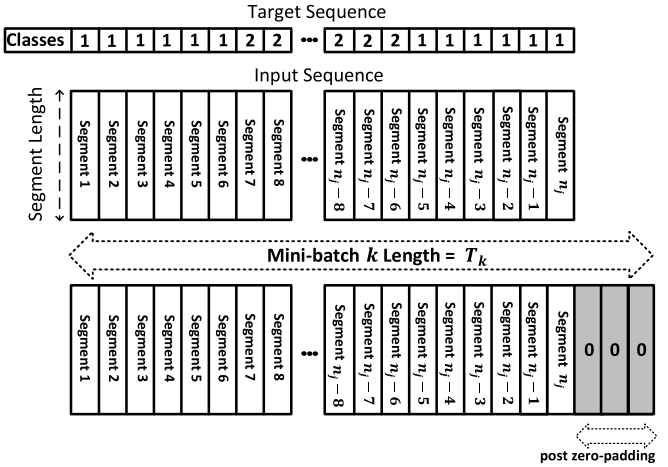

Fig. 2. Forming the input and output sequences using the segmented data.

E. Forming a Seq-to-Seq Classification Problem

Each segment derived from every KS sequence was labeled as: 1) after-systolic and before-diastolic (AB) and 2) before-systolic or after-diastolic (BA). Defining BA $= 1$ and AB $= 2$, the output target for the ith segment can be written as $y_i \in \{1, 2\}$. Let us assume that the jth segmented KS sequence consists of n_j segments. The target sequence for this sample can then be represented as $Y_j = [y_1, y_2, \ldots, y_{n_j}]$. Using the segments obtained from the KSs, we form the inputs (sequences of segments from the KSs) for the deep-learning model; Fig. 2 visualizes this. Having the sequences of segments derived from KSs and the corresponding target label sequences, as the first step to estimate SBP and DBP from KSs,

we formed a seq-to-seq classification problem which was dealt with the devised CNN-BiLSTM-RNN model explained in what follows in this section. It should be noted that the SBP and DBP were found from the sequences of labels as follows.

F. BP Estimation From Sequence of Labels

To estimate SBP and DBP from the sequence of labels, we first identified the segments at which the output target sequence, detected via the proposed deep-learning method, switches from class BA to class AB, and later from class AB to class BA. The SBP and DBP were then obtained as the CP values associated with the center point of the switching segments. In other words, we found the SBP and DBP by mapping the center point of the switching segments to the deflation curve associated with the collected KSs. Fig. 1 illustrates the diagram of the developed AI-based NIBP estimation method.

G. Network Architecture Used to Solve the Seq-to-Seq Classification Problem

This article proposes a new end-to-end DNN classification model for BP estimation from sequences of KSs. This model comprises both recurrent and convolutional layers. The convolutional layers were used to extract features from signal segments, and the recurrent (BiLSTM) layers were used to model the temporal dynamics in the feature maps.

A feature map using a 1-D convolution operation can be formulated as

$$x_m^{(l+1)}(\tau) = \mathrm{ELU}\left(b_m^l + \sum_{i=1}^{S_l} K_{mi}^l(\tau) * x_i^l(\tau)\right) = \mathrm{ELU}\left(b_m^l + \sum_{i=1}^{S_l}\sum_{q=1}^{Q_l} K_{mi}^l(q) x_i^l(\tau - q)\right) \quad (1)$$

where x_m^l, S_l, b_m^l, and Q_l denote the feature map m, the number of feature maps, the bias, and the length of kernels, respectively, in the lth layer. Additionally, K_{mi}^l represents the kernel convolved over the feature map i in the lth layer to generate the feature map m in the layer $l+1$ and ELU means exponential linear unit which computes the function

$$f(x) = \begin{cases} x, & x > 0 \\ \alpha(e^x - 1), & x \le 0 \end{cases} \quad (2)$$

where $\alpha > 0$ is the scale for the negative factor, and in this study, was set to 1. The stride length used here is 1, that is, the kernels were always shifted by one sample.

Features extracted using CNN layers are passed to bidirectional LSTM-RNNs (BiLSTM-RNNs) [35], which can process the data sequence in both forward and backward directions using two separate recurrent layers. These layers are then merged into the same output layer, that is,

$$h_t^f = \mathscr{H}\left(x_t, h_{t-1}^f, W^f\right) \quad h_t^b = \mathscr{H}\left(x_t, h_{t-1}^b, W^b\right) \quad (3)$$

where h_t^b and h_t^f denote the backward and forward hidden states, respectively, W^b and W^f represent the corresponding weights, and $\mathscr{H}(\cdot,\cdot,\cdot)$ refers to the LSTM unit formulation [36]. The output of the hidden layer of a BiLSTM-RNN, h, is achieved by concatenating the two unidirectional LSTM layers' outputs as $h_t = \mathrm{concat}(h_t^f, h_t^b)$. The output probabilities $\hat{y}$ are obtained as

$$\hat{y}_t = \sigma(b_t + W_z h_t). \quad (4)$$

In this study, for training the proposed deep-learning-based model, we used the back-propagation algorithm to minimize the cross-entropy below

$$J = -\sum_{i=1}^{N_m}\sum_{t=1}^{T_k} y_t(\log\ \hat{y}_t(W,b)) + \gamma\,\|\xi\| \quad (5)$$

where $\hat{y}_t(W,b)$ and y_t are the predicted probability of the output and the target output, respectively, corresponding to the input x_t, and N_m denotes the mini-batch size. In the above index function, $\|\cdot\|$ denotes the L_2 norm and ξ represents the model parameters, and γ is the penalty coefficient. Besides, T_k represents the length of zero-padded sequences in the kth mini-batch. Note that $k = 1, \ldots, (N_{tr}/N_m)$, where N_{tr} represents the training data size.

In this study, we used a fivefold cross-validation method, that is, the dataset was randomly split into five subsets each of which included 70 samples, and in each run, four subsets were used for training the deep-learning model, and a subset was used as the test dataset. Although the number of features extracted from each segment using the CNN is identical for each sample, the number of segments derived from different KS samples and thus the lengths of the resulting input sequences would not be fixed. Therefore, as the input to the devised network must be a tensor with fixed dimensions, we divided the training data into a number of subsets (mini-batches) and further post zero-padded the sequences within each mini-batch (see Fig. 2). Furthermore, if samples in a mini-batch have very different lengths, the zero-padding required to make their lengths identical can have a negative impact on the model performance. To overcome this, in this study, it was attempted to accumulate the sequences with a relatively similar length in a mini-batch. To this end, we sorted the training samples (i.e., $N_{tr} = 280$) based on their size and divided them into subsets of size $N_m = 10$ (i.e., mini-batch size was 10) to ensure that the sequences in each mini-batch were of the relatively similar length and thus the zero-padding used to make their length identical was modest. The so-called masking technique [37] was also used to ignore the padded time steps during the loss calculations.

The structure of the developed CNN-BiLSTM model is depicted in Figs. 1 and 3. As it is shown in Fig. 3, the first layer in the proposed CNN is a special layer obtained by concatenating three convolution layers with kernel sizes of 3, 4, and 5, each of which included three kernels. The kernel size of the following convolutional layers is 3. The number of kernels in the first three convolutional layers after the depth concatenation layer and the rest of the layers is 12 and 24, respectively. Moreover, there are skip architectures in the proposed network. In Block A, a global pooling strategy is obtained by subtracting the output of global-average-pooling (taking the average value per features map)

TABLE II

HYPERPARAMETERS OF THE DEVISED CNN-BILSTM

Hyper-parameter	Value/Method
Mini-batch size	10
Epochs	50
Dropout rate in recurrent layers	0.1
Dropout rate in CNN	0.1
L_2 regularization factor	0.0001
Optimization algorithm	Adam
Gradient decay factor	0.9000
Squared gradient decay factor	0.9990
Initial learning rate	0.001

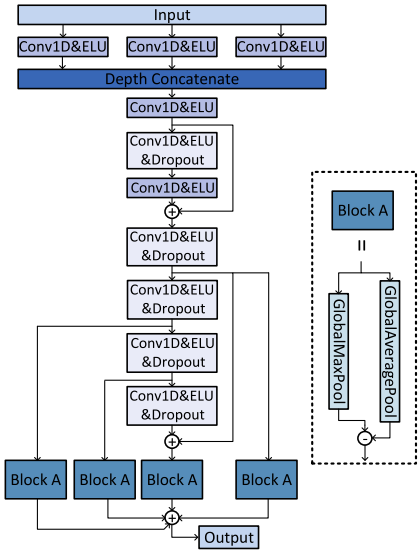

Fig. 3. Proposed CNN architecture for feature extraction from segments of KSs.

from the output of global-max-pooling (taking the maximum per features map). To prevent overfitting, dropout layers with a rate of 0.1 (i.e., at each update of the training phase 10% of the outgoing edges of hidden units are randomly set to 0) are also used in this structure.

III. RESULTS

The results reported here are the average of the five values yielded from five different test sample sets. We tuned the hyperparameters of the devised CNN-BiLSTM using extensive experiments on 80% of the NIBP samples and validated on the remaining 20% of samples, as shown in Table II. Hence, the sensitivity of the achieved results to the tuned hyperparameters is modest.

In this study, we tested ten different models that used CNN architecture in Fig. 3 for feature extraction, with the structures/parameters presented in Table III. Table IV presents the results obtained from different models using different segmentation methods.

As highlighted in Table IV, the best results were achieved by the proposed CNN-BiLSTM model using the second segmentation technique that provided sequences of segments with a length of 501 samples to the DL model. Besides, among the models trained on the sequences of segments generated by the first segmentation technique, that is, the sliding window technique, Model 6, which used sequences of segments with

TABLE III

STRUCTURE OF DIFFERENT CONVOLUTIONAL NEURAL NETWORK-BASED MODELS TESTED IN THIS STUDY

Model	Segmentation Method	Window Length (samples)	Overlap (samples)	Classification Layer
Model 1	Second	501	NA	BiLSTM
Model 2	first	1000	500	BiLSTM
Model 3	first	750	250	BiLSTM
Model 4	first	500	200	BiLSTM
Model 5	first	350	150	BiLSTM
Model 6	first	250	100	BiLSTM
Model 7	first	150	50	BiLSTM
Model 8	first	250	0	BiLSTM
Model 9	first	250	100	LSTM
Model 10	first	250	100	Dense

BiLSTM: Bidirectional Long-Short-Term-Memory; NA: not applicable. BiLSTM layers in Models 1-8 included 2*75 units, LSTM layer in Model 9 included 75 units, and the dense layer in Model 10 included 75 neurons. The segmentation methods are described in Section II-D.

a length of 250 samples with an overlap of 100 achieved the best results.

To check that the results achieved by the fivefold cross-validation scheme will generalize to independent datasets, another cross-validation scheme was used as well; leave-one-fifth-of-subjects-out CV (LOFOSOCV). This CV scheme was used to check that the achieved results are subject-independent and was carried out by keeping all the samples from 20% of subjects for validation and using the rest for training. As seen from Table IV, the achieved results by these two CV schemes are very close to the ones achieved by the fivefold CV scheme.

Table IV further presents the results achieved by the unidirectional LSTM network and beat-by-beat time-domain handcrafted features proposed in [31].

IV. DISCUSSION

As evident from Table IV, Model 1, that is, a CNN-BiLSTM model trained by segments of KSs obtained by the second proposed segmentation technique, which requires the estimation of the cardiac period, achieves the best results. Table IV further reveals that, among the models using inputs derived from the sliding segmentation technique with or without overlap, Model 6, that is, a CNN-BilSTM network trained by inputs from a sliding segmentation technique with a window width of 250 samples and an overlap of 100 samples, achieved the best results. While this model gave relatively less accurate results in regard to mean absolute error (MAE) and SDE compared to Model 1, an advantage of this approach is that it does not require the estimation of the cardiac period. It can also be seen from Table IV that on average the absolute error of SBP estimation using Model 6 in 91% of cases was $\leq$5 mmHg, while Model 1 only in 86.7% of cases could estimate SBP with an absolute error of $\leq$5 mmHg. On the other hand, the absolute error of 2.5% of the SBP estimates was more than 15 mmHg with Model 6, while this rate was about 1.7% with Model 1. This can explain why the SDE and MAE achieved by Model 6 were relatively higher than Model 1. Furthermore, as seen, by reducing the sliding window's width down to 250 samples, the accuracy of the seq-to-seq deep-learning-based method developed for BP estimation increases. It is also noted that a window width of 150 samples could

TABLE IV

RESULTS ACHIEVED BY DIFFERENT DEEP-LEARNING-BASED MODELS, WITH THE DETAILS GIVEN IN TABLE III, EXAMINED FOR SYSTOLIC AND DIASTOLIC BLOOD PRESSURE ESTIMATION FROM KS SEQUENCES. BOLD ENTRIES INDICATE THE BEST ACHIEVED RESULTS

Classification Method	Absolute Difference (%) ≤ 5	≤ 10	≤ 15	ME (mmHg)	MAE (mmHg)	SDE (mmHg)	BHS Grade	AAMI Standard
Systolic Blood Pressure								
Model 1*	**86.7**	**95.7**	**98.3**	**-0.5**	**1.6**	**3.9**	**A**	**Pass**
Model 1 With LOFOSOCV	88.4	95.7	98.0	0.4	1.6	4.1	A	Pass
Model 2	76.3	94.9	98.0	1.0	3.9	4.7	A	Pass
Model 3	80.0	94.6	97.7	0.7	3.4	4.9	A	Pass
Model 4	83.0	97.6	98.6	0.3	2.8	4.5	A	Pass
Model 5	88.6	94.9	97.7	1.1	2.7	4.5	A	Pass
Model 6**	**91.0**	**96.3**	**97.5**	**0.7**	**2.3**	**4.2**	**A**	**Pass**
Model 7	88.0	94.9	96.6	0.9	2.8	8.0	A	Fail
Model 8	86.6	94.9	98.0	-0.4	2.4	4.8	A	Pass
Model 9	82.0	86.9	90.3	2.9	5.6	12.8	B	Fail
Model 10	78.9	88.0	92.0	1.7	5.9	13.9	B	Fail
LSTM with features from KSs in [31]	79.7	92.3	96.0	-1.7	2.5	4.8	A	Pass
LSTM with features extracted from OW in [14]	64.1	90.0	97.1	-1.2	3.8	5.9	A	Pass
FFNN classification with features extracted from OW in [14]	70.1	92.8	96.8	0.9	3.2	6.1	A	Pass
FFNN regression with features extracted from OWE in [38]	58.5	80.5	91.1	0.6	6.7	10.9	B	Fail
MAA [39], [40]	40.7	59.9	79.1	0.1	9.6	13.4	D	Fail
MMSA [12]	39.0	63.3	81.7	4.4	9.1	11.5	D	Fail
Diastolic Blood Pressure								
Model 1*	**82.0**	**96.3**	**99.4**	**0.7**	**2.5**	**4.0**	**A**	**Pass**
Model 1 With LOFOSOCV	80.0	95.8	98.9	1.0	2.9	4.4	A	Pass
Model 2	72.4	94.0	99.2	-1.0	3.6	4.8	A	Pass
Model 3	78.9	94.9	99.4	-0.1	3.2	4.4	A	Pass
Model 4	79.7	94.6	99.6	0.1	2.9	4.2	A	Pass
Model 5	78.0	95.7	99.1	-0.5	3.1	4.3	A	Pass
Model 6**	**82.0**	**94.6**	**99.4**	**-0.4**	**2.8**	**4.2**	**A**	**Pass**
Model 7	80.3	95.7	98.3	-0.2	3.1	4.6	A	Pass
Model 8	80.9	96.3	99.1	-0.1	2.9	4.3	A	Pass
Model 9	75.4	92.9	98.9	0.1	3.6	4.8	A	Pass
Model 10	51.1	66.0	77.7	-5.1	9.9	14.3	D	Fail
LSTM with features from KSs in [31]	63.7	84.7	95.9	1.6	3.9	6.6	A	Pass
LSTM with features extracted from OW in [14]	40.0	71.3	91.7	1.8	7.2	8.8	D	Fail
FFNN classification with features extracted from OW in [14]	42.3	69.1	88.6	2.7	7.2	9.5	C	Fail
FFNN regression with features extracted from OWE in [38]	34.7	63.6	80.5	-0.1	9.0	11.4	D	Fail
MAA [39], [40]	28.4	55.3	77.1	1.2	10.8	14.4	D	Fail
MMSA [12]	25.8	47.3	65.6	10.7	12.9	12.8	D	Fail

* indicates the best result; ** indicates the best results archived using the first segmentation technique; MAE: Mean Absolute Error; SDE: Standard Deviation of Error; ME: Mean Error; AAMI: Association for the Advancement of Medical Instrumentation; BHS: British Hypertension Society; LOFOSOCV: leave-one-fifth-of-subjects-out cross validation; FFNN: feedforward neural network; LSTM: long-short-term-memory; MAA: maximum amplitude algorithm; MMSA: maximum/minimum slope algorithm; OW: oscillometric waveform; OWE: oscillometric waveform envelop; KSs: Korotkoff sounds.

not achieve a good result. This can be explained by the fact that a small window width may not cover the gap between two consecutive pulses even when a sliding window with overlap segmentation was used, and as a result, the continuity of the resulting input sequence cannot be guaranteed for KSs collected during very low heart rates.

The results reported in Table IV also demonstrate that, for DBP estimation, all the models tested could provide a Grade A performance (BHS protocol) and could meet the AAMI protocol, except Model 10 in which the BiLSTM layer was replaced with a dense layer. For SBP estimation, only the networks with a BiLSTM layer resulted in a BHS Grade A and provided acceptable results based on the AAMI protocol. It should be highlighted that the models using unidirectional LSTM layers could not provide a BHS Grade A for SBP estimation or equivalently could not estimate SBP accurately. The low accuracy of the models without the BiLSTM layer can be explained by the fact that these models are unable to detect the segment associated with the systolic pressure in the presence of noise in the presystolic phase, as an unidirectional LSTM layer does not have access to the future information and hence cannot avoid misclassification of a noise as a KS. The achieved results further highlight the fact that the most accurate results could be achieved by the models that (1) assume that the segments derived from KSs are temporally dependent and take into account these temporal dependencies when classifying a segment, and additionally (2) use both future and past information of the segment sequences achieved from segmentation of KSs to detect the segments associated with SBP and DBP. It should also be noted that the output layer of the networks with the BiLSTM layer receives both the future and past information for every segment and more importantly, the inputs are not displaced from their relevant targets. Hence, these models can detect the segments associated with the SBP and DBP more accurately when the collected KS signals are noisy.

Bland–Altman plots [41] in Fig. 4 compare the best results achieved by the developed CNN-BiLSTM-RNN (Model 1) with the reference values. These plots show the results achieved on the five test subsets. It is evident from these

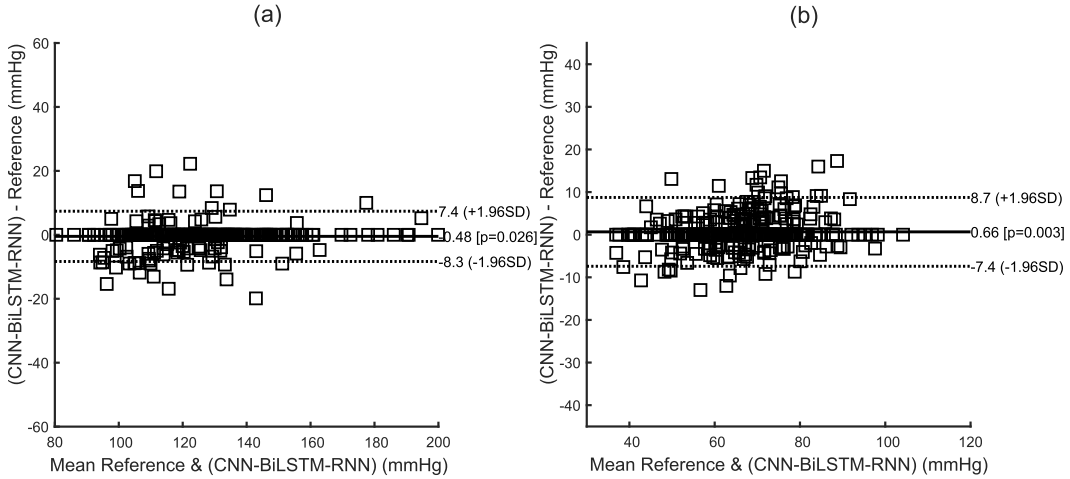

Fig. 4. Bland–Altman plots comparing the output of Model 1, a CNN-BiLSTM-RNN model trained by segments of KSs obtained by the second proposed segmentation technique which requires the estimation of the cardiac period, versus gold reference values for (a) systolic and (b) diastolic BPs.

Bland–Altman plots that the proposed method can accurately estimate SBP and DBP, as most black squares are within the dotted horizontal lines (i.e., limits of agreement: ME $\pm$ 1.96 $\times$ SDE).

The current data-driven-based methods for BP estimation from KSs suffer from two major problems. First, algorithms that classify every segment derived from KSs independent of other segments, ignore the temporal dependencies between segments obtained from KSs (cf., [27]). Second, algorithms that use unidirectional LSTM-RNNs [31] or other models that can be used for seq-to-seq classification problems, for example, GMM-HMMs [30], can only label each feature vector extracted from a segment based on the previous information. Hence, they cannot deal with noise in KSs that happens before the systolic point.

Another limitation of the current data-driven-based methods introduced for NIBP estimation from KSs is that, in these methods, the segmentation of the KSs requires that a parallel OW is present. Specifically, to carry out the segmentation of KSs, the location of each oscillometric peak is used as the center point for each segment (cf. [27], [37]). In this study, we alternatively developed and used two more advanced segmentation techniques that can segment the KSs without OWs. This further eliminates the need for the preprocessing step required to find the location of oscillometric peaks. Furthermore, in this study, we developed a CNN with a special structure trained to extract optimal features from segments of KSs. This approach is quite different from the current methods that use manual feature extraction techniques (cf. [30], [31]) and requires less preprocessing steps to process the raw data and provide suitable inputs for the classification algorithm.

While oscillometric methods are now the most popular NIBP means of estimating SBP and DBP, all these methods are calibrated using the auscultatory method and KSs as set by the international standards bodies (AAMI/ESH/ISO). Improving the accuracy of Korotkoff-based methods will thus have an impact on the performance of all NIBP devices. It was shown in [24] and [25] that the manual auscultatory technique can be inaccurate due to several reasons such as the hearing acuity of the observer, the sensitivity of the stethoscope employed, the morphology and intensity of the KS, the patient's anatomy, and the indistinct or unclear KSs at systolic and diastolic points. The end-to-end deep-learning-based NIBP estimation method developed in this study can overcome these drawbacks and estimate BP more accurately, as it processes the digitized KSs rather than auscultation of KSs and thus can 1) detect indistinct KSs at SBP and DBP and 2) recognize the difference between a real KS and noise.

As shown in [42], the highest frequency component of KSs can be close to 400 Hz but with very low energy. However, phases I and IV (and V), corresponding to systolic and diastolic beats, respectively, are related to the appearance and disappearance of the high-frequency component, namely K_2 [26], have frequencies less than 250 and 100 Hz, respectively. Although the transducer used in this study to record KSs did not have a wide frequency response similar to the one used in [26], its frequency response was sufficient for the detection of systolic and diastolic beats. The high-pass filter ($\geq$20 Hz) we used removed low-frequency components, namely K_1 and K_3, and although the remaining signal did not exactly resemble K_2 component of KSs, it was sufficient for the goal of this study.

The total number of trainable parameters in the proposed model (with a segment length of 501 samples) is 67 549. Also, we used an Intel(R) Core(TM) i7-9750H CPU @ 2.60 GHz to train the model. The trained deep-learning model can be run on microcontrollers or microcomputers, and we are currently developing an AI-based NIBP monitoring device using microcontrollers. A provisional patent (P0027996AU) has been granted to facilitate the development of new NIBP devices based on these and other developments.

Existing protocols for assessment of the accuracy of NIBP monitors exclude people with atrial fibrillation, except in certain circumstances [43]. Moreover, when a cardiac arrhythmia is present, current guidelines for hypertension diagnosis advise manual auscultatory NIBP measurement with repeated measurements to compensate for the increased beat-to-beat NIBP variability. On the other hand, the promoted method for

hypertension diagnosis is at-home NIBP monitoring that essentially requires automated devices [44]. Nevertheless, as shown by few studies undertaken on the accuracy of automated NIBP measurement in the presence of atrial fibrillation, none of the marketed oscillometric NIBP monitors is in full accordance with the current protocols [45]. As the developed deep-learning-based NIBP measurement technique in this study uses KSs as input, it can be an alternative algorithm for the development of automated NIBP monitoring devices that can be used in arrhythmia. The validation of the accuracy of the proposed method in the presence of arrhythmia will be the subject of our future work.

A. Study Limitations

In this study, we used a dataset of 350 NIBP recordings collected from a diverse population, following the recommendations of the standards bodies. However, more recordings from a more diverse population can make it possible to develop a more generalizable model. We also emphasized in a review paper [9] that "along with the development of novel AI-based methods for accurate NIBP estimation, future research needs to focus on validating and comparing existing models, using a unique large dataset with different invasive BP and NIBP samples with and without abnormalities such as measurement noise, cardiac arrhythmia, or signal artifact, so that the advantages and disadvantages of these models can be investigated. This makes it possible to check whether the existing models are sufficient or novel AI-based (deep learning) models should still be developed to achieve better results."

V. Conclusion

This study was devoted to the development of an end-to-end deep-learning-based algorithm for NIBP estimation from the sequences of KSs. Different from the current methods, to estimate NIBP from KSs, first, a seq-to-seq classification problem was formed, and a deep-learning-based algorithm was then developed to deal with this problem. The systolic and diastolic pressures were subsequently estimated by projecting the center of segments at which the detected label sequence changes from one class to another class, that is, before systolic or after diastolic to after systolic and before diastolic, and vice versa, to the corresponding cuff pressure curve. To the best of the authors' knowledge, this is the first end-to-end deep-learning-based algorithm developed for NIBP estimation from KSs. The proposed classification method is able to extract features from segments of KSs, achieved by segmentation of the KSs, without external intervention, and furthermore, unlike the existing methods, is capable of using both past and future context, thereby dealing with noise in the digitized KSs. The trained model can be ported into a portable NIBP monitor that is able to record KSs and can give highly accurate estimates of SBP and DBP.

References

[1] GBD 2017 Risk Factor Collaborators, "Global, regional, and national comparative risk assessment of 84 behavioural, environmental and occupational, and metabolic risks or clusters of risks for 195 countries and territories, 1990–2017: A systematic analysis for the global burden of disease study 2017," *Lancet*, vol. 392, no. 10159, pp. 1923–1994, Nov. 2018, doi: 10.1016/S0140-6736(18)32225-6.

[2] M. H. Olsen et al., "A call to action and a lifecourse strategy to address the global burden of raised blood pressure on current and future generations: The lancet commission on hypertension," *Lancet*, vol. 388, no. 10060, pp. 2665–2712, 2016.

[3] J. E. Sharman et al., "Lancet commission on hypertension group position statement on the global improvement of accuracy standards for devices that measure blood pressure," *J. Hypertension*, vol. 38, no. 1, pp. 21–29, 2020.

[4] R. Padwal et al., "Optimizing observer performance of clinic blood pressure measurement: A position statement from the lancet commission on hypertension group," *J. Hypertension*, vol. 37, no. 9, pp. 1737–1745, 2019.

[5] G. S. Stergiou et al., "A universal standard for the validation of blood pressure measuring devices: Association for the advancement of medical instrumentation/European society of hypertension/international organization for standardization (AAMI/ESH/ISO) collaboration statement," *Hypertension*, vol. 71, no. 3, pp. 368–374, 2018.

[6] B. V. Scheer, A. Perel, and U. J. Pfeiffer, "Clinical review: Complications and risk factors of peripheral arterial catheters used for haemodynamic monitoring in anaesthesia and intensive care medicine," *Crit. Care*, vol. 6, no. 3, pp. 198–204, 2002.

[7] S. Hunyor, J. Flynn, and C. Cochineas, "Comparison of performance of various sphygmomanometers with intra-arterial blood-pressure readings," *Br Med. J.*, vol. 2, no. 6131, pp. 159–162, Jul. 1978.

[8] S. Breit and M. O'Rourke, "Comparison of direct and indirect arterial pressure measurements in hospitalised patients," *Austral. New Zealand J. Med.*, vol. 4, no. 5, pp. 485–491, Oct. 1974.

[9] A. Argha, B. G. Celler, and N. H. Lovell, "Artificial intelligence based blood pressure estimation from auscultatory and oscillometric waveforms: A methodological review," *IEEE Rev. Biomed. Eng.*, vol. 15, pp. 152–168, 2020.

[10] M. Forouzanfar, H. R. Dajani, V. Z. Groza, M. Bolic, S. Rajan, and I. Batkin, "Oscillometric blood pressure estimation: Past, present, and future," *IEEE Rev. Biomed. Eng.*, vol. 8, pp. 44–63, 2015.

[11] K.-G. Ng and C. F. Small, "Survey of automated noninvasive blood pressure monitors," *J. Clin. Eng.*, vol. 19, no. 6, pp. 452–475, Nov. 1994.

[12] G. Drzewiecki and J. D. Bronzino, "Noninvasive arterial blood pressure and mechanics," in *The Biomedical Engineering Handbook*, vol. 1. Boca Raton, FL, USA: CRC Press, 2000, pp. 1–16.

[13] M. Mafi, M. Bolic, V. Z. Groza, H. R. Dajani, and S. Rajan, "Oscillometric blood pressure pulse morphology," in *Proc. IEEE Int. Symp. Med. Meas. Appl.*, May 2011, pp. 413–417.

[14] A. Argha and B. G. Celler, "Blood pressure estimation from time-domain features of oscillometric waveforms using long short-term memory recurrent neural networks," *IEEE Trans. Instrum. Meas.*, vol. 69, no. 6, pp. 3614–3622, Jun. 2020.

[15] B. G. Celler, P. N. Le, A. Argha, and E. Ambikairajah, "GMM-HMM-based blood pressure estimation using time-domain features," *IEEE Trans. Instrum. Meas.*, vol. 69, no. 6, pp. 3631–3641, Jun. 2020.

[16] A. Argha, J. Wu, S. W. Su, and B. G. Celler, "Blood pressure estimation from beat-by-beat time-domain features of oscillometric waveforms using deep-neural-network classification models," *IEEE Access*, vol. 7, pp. 113427–113439, 2019.

[17] R. Mukkamala et al., "Evaluation of the accuracy of cuffless blood pressure measurement devices: Challenges and proposals," *Hypertension*, vol. 78, no. 5, pp. 1161–1167, 2021.

[18] B. G. Celler, A. Argha, P. N. Le, and E. Ambikairajah, "Novel methods of testing and calibration of oscillometric blood pressure monitors," *PLoS ONE*, vol. 13, no. 8, Aug. 2018, Art. no. e0201123.

[19] M. Alvarado Alvarez, R. Padwal, J. Ringrose, A. Jalali, and W. Hiebert, "Optimum waveform envelopes and amplitude ratios in oscillometric blood pressure estimation," *Blood Pressure Monitor.*, vol. 26, no. 1, pp. 53–59, Feb. 2021.

[20] A. K. Gupta, A. Maheshwari, D. D. Tresch, and R. K. Thakur, "Cardiac arrhythmias in the elderly," *Cardiac Electrophysiol. Rev.*, vol. 6, nos. 1–2, pp. 120–128, Feb. 2002.

[21] M. J. Cleland, B. Pham, and D. R. Miller, "Influence of arrhythmias on accuracy of non-invasive blood pressure monitors," *Can. J. Anaesthesia*, vol. 45, no. 7, pp. 699–705, Jul. 1998.

[22] B. S. Alpert, "The accutension stetho, an automated auscultatory device to validate automated sphygmomanometer readings in individual patients," *J. Hum. Hypertension*, vol. 32, pp. 455–459, Apr. 2018.

[23] G. Chu, Z. Zhang, M. Xu, D. Huang, and Q. Dai, "Validation of a smartphone auscultatory blood pressure kit accutension XYZ-110 in adults according to the ANSI/AAMI/ISO 81060–2: 2013 standard," *Blood Pressure Monitor.*, vol. 22, no. 5, pp. 290–294, 2017.

[24] B. G. Celler, P. Le, J. Basilakis, and E. Ambikairajah, "Improving the quality and accuracy of non-invasive blood pressure measurement by visual inspection and automated signal processing of the Korotkoff sounds," *Physiolog. Meas.*, vol. 38, no. 6, pp. 1006–1022, Jun. 2017.

[25] D. Zheng, R. Giovannini, and A. Murray, "Effect of respiration, talking and small body movements on blood pressure measurement," *J. Human Hypertension*, vol. 26, no. 7, pp. 458–462, Jul. 2012.

[26] S. G. Blank et al., "Wideband external pulse recording during cuff deflation: A new technique for evaluation of the arterial pressure pulse and measurement of blood pressure," *Circulation*, vol. 77, no. 6, pp. 1297–1305, 1988.

[27] F. Pan, P. He, C. Liu, T. Li, A. Murray, and D. Zheng, "Variation of the Korotkoff stethoscope sounds during blood pressure measurement: Analysis using a convolutional neural network," *IEEE J. Biomed. Health Informat.*, vol. 21, no. 6, pp. 1593–1598, Nov. 2017.

[28] F. Pan, P. He, F. Chen, J. Zhang, H. Wang, and D. Zheng, "A novel deep learning based automatic auscultatory method to measure blood pressure," *Int. J. Med. Informat.*, vol. 128, pp. 71–78, Aug. 2019.

[29] J.-H. Chang and I. Doh, "Deep learning-based robust automatic non-invasive measurement of blood pressure using Korotkoff sounds," *Sci. Rep.*, vol. 11, no. 1, pp. 1–12, Dec. 2021.

[30] B. G. Celler, P. N. Le, A. Argha, and E. Ambikairajah, "Blood pressure estimation using time domain features of auscultatory waveforms and GMM-HMM classification approach," in *Proc. 41st Annu. Int. Conf. IEEE Eng. Med. Biol. Soc. (EMBC)*, Jul. 2019, pp. 208–211.

[31] A. Argha and B. G. Celler, "Blood pressure estimation using time domain features of auscultatory waveforms and deep learning," in *Proc. 41st Annu. Int. Conf. IEEE Eng. Med. Biol. Soc. (EMBC)*, Jul. 2019, pp. 1821–1824.

[32] *American National Standards for Electronic or Automated Sphygmomanometers*, Standards ANSI/AAMI SP 10, 1987.

[33] E. O'Brien et al., "The British hypertension society protocol for the evaluation of blood pressure measuring devices," *J. Hypertension*, vol. 11, pp. 43–62, Jun. 1993.

[34] O. Banos, J.-M. Galvez, M. Damas, H. Pomares, and I. Rojas, "Window size impact in human activity recognition," *Sensors*, vol. 14, no. 4, pp. 6474–6499, 2014.

[35] M. Schuster and K. K. Paliwal, "Bidirectional recurrent neural networks," *IEEE Trans. Signal Process.*, vol. 45, no. 11, pp. 2673–2681, Nov. 1997.

[36] S. Hochreiter and J. Schmidhuber, "Long short-term memory," *Neural Comput.*, vol. 9, no. 8, pp. 1735–1780, 1997.

[37] A. Argha, B. G. Celler, and N. H. Lovell, "A novel automated blood pressure estimation algorithm using sequences of Korotkoff sounds," *IEEE J. Biomed. Health Informat.*, vol. 25, no. 4, pp. 1257–1264, Apr. 2021.

[38] M. Forouzanfar, H. R. Dajani, V. Z. Groza, M. Bolic, and S. Rajan, "Feature-based neural network approach for oscillometric blood pressure estimation," *IEEE Trans. Instrum. Meas.*, vol. 60, no. 8, pp. 2786–2796, Aug. 2011.

[39] D. Zheng, J. N. Amoore, S. Mieke, and A. Murray, "Estimation of mean arterial pressure from the oscillometric cuff pressure: Comparison of different techniques," *Med. Biol. Eng. Comput.*, vol. 49, no. 1, pp. 33–39, Jan. 2011.

[40] M. Forouzanfar, S. Ahmad, I. Batkin, H. R. Dajani, V. Z. Groza, and M. Bolic, "Coefficient-free blood pressure estimation based on pulse transit time–cuff pressure dependence," *IEEE Trans. Biomed. Eng.*, vol. 60, no. 7, pp. 1814–1824, Jul. 2013.

[41] J. M. Bland and D. G. Altman, "Comparing methods of measurement: Why plotting difference against standard method is misleading," *Lancet*, vol. 346, no. 8982, pp. 1085–1087, Oct. 1995.

[42] J. Allen, T. Gehrke, J. J. O'Sullivan, S. T. King, and A. Murray, "Characterization of the Korotkoff sounds using joint time–frequency analysis," *Physiolog. Meas.*, vol. 25, no. 1, pp. 107–117, Feb. 2004.

[43] E. O'Brien et al., "European society of hypertension international protocol revision 2010 for the validation of blood pressure measuring devices in adults," *Blood Pressure Monitor.*, vol. 15, no. 1, pp. 23–38, 2010.

[44] *Hypertension: Clinical Management of Primary Hypertension in Adults*, National Institute for Health and Clinical Excellence, London, U.K., 2011.

[45] C. E. Clark, S. T. J. McDonagh, and R. J. Mcmanus, "Accuracy of automated blood pressure measurements in the presence of atrial fibrillation: Systematic review and meta-analysis," *J. Hum. Hypertension*, vol. 33, no. 5, pp. 352–364, May 2019.

Ahmadreza Argha (Member, IEEE) received the B.Sc. and M.Sc. degrees in electrical engineering from Shiraz University, Shiraz, Iran, in 2003 and 2006, respectively, and the Ph.D. degree from the University of Technology Sydney (UTS), Ultimo, NSW, Australia, in 2017.

He is currently a Post-Doctoral Research Fellow with the Graduate School of Biomedical Engineering, University of New South Wales (UNSW), Sydney, NSW. His current research interests include data analytics especially related to telehealth technologies, biological signal processing, and machine-learning and deep-learning applications in biomedical engineering.

Branko G. Celler (Life Fellow, IEEE) received the B.Sc. degree in physics and computer science, the B.E.E. degree (major in control), and the Ph.D. degree in biomedical engineering from the University of New South Wales (UNSW), Sydney, NSW, Australia, in 1969, 1971, and 1978, respectively.

He subsequently completed a Post-Doctoral Fellowship with the Johns Hopkins School of Medicine, Baltimore, MD, USA, in 1980, before returning to Australia to take up an academic position at the UNSW. He established and led the Biomedical Systems Laboratory, School of Electrical Engineering and Telecommunications, UNSW, from 1981 to 2006, and was appointed as a Full Professor in 1997 and was the Head of the School from 1998 to 2006. He has published over 300 refereed journal articles and conference proceedings as well as 14 book chapters and has received more than $15m in competitive national research funding. His research interests include biomedical instrumentation and signal processing, bioinformatics, and decision support systems as applied to telehealth systems for the management of chronic disease in the home and the community.

Hamid Alinejad-Rokny (Member, IEEE) received the Ph.D. degree in systems biology and machine learning from the University of New South Wales (UNSW), Sydney, NSW, Australia, in 2018.

He is currently the Team Leader of the UNSW BioMedical Machine Learning Laboratory (BML), Graduate School of Biomedical Engineering, UNSW. His research focuses on using cutting-edge systems biology and artificial intelligence techniques to understand the genomic and transcriptomic signals in genetic diseases and cancers.

Nigel H. Lovell (Fellow, IEEE) is currently with the Graduate School of Biomedical Engineering, University of New South Wales (UNSW), Sydney, NSW, Australia, where he holds a position of Scientia Professor and the Head of School. His research work has covered areas of expertise ranging from cardiac and retinal modeling, to medical informatics, and data analytics, especially related to telehealth technologies, biological signal processing, and visual prosthesis design. Much of his work has been in the design of appropriate technologies to restore sensory loss and manage chronic disease and frailty. He has commercialized a range of telehealth technologies for managing chronic disease and falls in the older population.

Prof. Lovell has been awarded over $84 million in research and development funding. Over his career, he has mentored 70 Ph.D. students and delivered more than a hundred keynote presentations. He is a fellow of seven learned academies and has been ranked as one of the top ten most published biomedical engineers in the world. In 2017 and 2018, he was the President of the world's largest biomedical engineering society—the IEEE Engineering in Medicine and Biology Society.